SCIENCE CHINA
Information Sciences

• RESEARCH PAPER •

July 2024, Vol. 67, Iss. 7, 172202:1–172202:16
https://doi.org/10.1007/s11432-023-3949-3

Adaptive neural network control of a 2-DOF helicopter system considering input constraints and global prescribed performance

Zhijia ZHAO[1], Jiale WU[1], Zhijie LIU[2*], Wei HE[2] & C. L. Philip CHEN[3,4]

[1]*School of Mechanical and Electrical Engineering, Guangzhou University, Guangzhou* 510006*, China;*
[2]*School of Intelligence Science and Technology and Key Laboratory of Intelligent Bionic Unmanned Systems of Ministry of Education, University of Science and Technology Beijing, Beijing* 100083*, China;*
[3]*School of Computer Science and Engineering, South China University of Technology, Guangzhou* 510641*, China;*
[4]*Pazhou Lab, Guangzhou* 510335*, China*

Received 26 May 2023/Revised 11 August 2023/Accepted 25 December 2023/Published online 25 June 2024

Abstract In this study, an adaptive neural network (NN) control is proposed for nonlinear two-degree-of-freedom (2-DOF) helicopter systems considering the input constraints and global prescribed performance. First, radial basis function NN (RBFNN) is employed to estimate the unknown dynamics of the helicopter system. Second, a smooth nonaffine function is exploited to approximate and address nonlinear constraint functions. Subsequently, a new prescribed function is proposed, and an original constrained error is transformed into an equivalent unconstrained error using the error transformation and barrier function transformation methods. The analysis of the established Lyapunov function proves that the controlled system is globally uniformly bounded. Finally, the simulation and experimental results on a constructed Quanser's test platform verify the rationality and feasibility of the proposed control.

Keywords adaptive NN control, 2-DOF helicopter, global prescribed performance, input constraints

1 Introduction

With the rapid development of science and technology, the unmanned aerial vehicles (UAVs) technology is gradually improving; in addition, it has been widely studied. As a typical UAV, the helicopter is not only characterized by low cost, small size, and strong survivability but is also simple in structure and convenient to use. It has been widely used in military reconnaissance and drone aircraft [1], civil aviation photography and express transportation [2], disaster relief [3], geographic mapping [4], and other fields. However, the helicopter is a nonlinear system with uncertainties and cross-coupling between the axes [5]. These characteristics cause significant challenges in the design of the controller. Therefore, an effective control method must be developed to overcome these challenges and guarantee the robustness of helicopter systems.

For the past few years, numerous control strategies have been designed to control the stability of helicopter systems. Kumar et al. [6] designed a state feedback controller based on a linear quadratic regulator (LQR) to achieve the angle position tracking of two-degree-of freedom (2-DOF) helicopters. Ref. [7] proposed a Q-learning control to stabilize 2-DOF helicopters with an unknown model by learning the optimal function from system data. In [8], a model-based LQR was proposed to track the desired trajectory of an unknown 2-DOF helicopter system. However, the above studies only considered the linearized system model and ignored the nonlinear term of helicopter systems, which may destabilize helicopter systems in practice. Therefore, in the design process of an efficient controller, the nonlinear aspect of helicopter systems should be considered.

Many control methods have been introduced to investigate the nonlinear characteristics of helicopter systems. Zou et al. [9] proposed a nonlinear robust control algorithm, which solved the singularity of

* Corresponding author (email: liuzhijie@ustb.edu.cn)

the tracking process using an attitude loop controller and verified it in a helicopter system. In [10], fuzzy control strategies were designed to optimize the dynamic tracking response of a helicopter system. In [11], a nonlinear controller was designed to solve the singular problem of roll angle, and the stability of the helicopter system with actuator fault was verified. However, the above studies assumed that the helicopter model was known and ignored the uncertainties of helicopter systems in the real situation. Therefore, uncertainties of nonlinear helicopter systems must be further explored.

In recent years, neural network (NN) control methods have been developed and widely used [12,13]. In particular, the radial basis function NN (RBFNN) is often exploited to consider the parameter uncertainty of nonlinear systems because of its simple structure and fast convergence. Yang et al. [14] designed an RBFNN control algorithm to estimate unknown functions in the system and verified it using a coupled motor drive. In [15], an RBFNN was used to explore the unknown dynamics model of a hexacopter UAV system and guarantee a consistent and stable attitude control based on events in finite time. In [16], an RBFNN was proposed for real-time estimation of a 3-DOF helicopter system with unmodeled dynamics, which was verified using effective tracking of attitude angles. In [17], an adaptive NN control method was designed, which used RBFNN to estimate the unknown dynamic model of helicopters and adaptively solved the unknown backlash-like hysteresis problem. In [18], an RBFNN control method was used to simultaneously solve the problems of system uncertainty and input backlash nonlinearity in a 2-DOF helicopter. The above studies attempted to explore the uncertainty of nonlinear systems. However, actual control systems are typically subjected to input constraints owing to the physical limitations of system components, which may degrade control performance and even cause system instability. Therefore, in the design of control systems, input constraints must be considered.

In practical conditions, the system input is affected by various constraints, including the saturation, hysteresis, and deadzone [19–21]. The input saturation is a factor that affects the stability of the system. Thus, many control algorithms have been developed to explore the input saturation constraint. Zhao et al. [22] established an adaptive NN controller for mobile manipulation subject and solved the actuator saturated input using an auxiliary system. Sedghi et al. [23] designed adaptive laws to estimate the unknown parameters of the input saturation of autonomous underwater vehicles to guarantee the trajectory tracking performance within a finite time. In [24], the RBFNN was exploited to approximate the saturation error and verify the stability of helicopter systems. In [25], a double closed-loop proportional differential (PD) control method was used to achieve the stable flight of a flapping-wing flying robot with input saturation. The above studies have significantly contributed to the investigations on input saturation constraints; however, the problem of prescribed performance of the output in practical applications cannot be neglected. A prescribed performance can reduce tracking errors and improve the system's transient response. Therefore, the prescribed performance must be considered in designing and implementing control methods for helicopter systems.

The prescribed performance control (PPC) was first proposed in [26], which guaranteed that the tracking error, convergence rate, and maximum overshoot always evolved within a prespecified range [27–29]. Recently, the PPC method has yielded significant achievements, and many findings have been reported in this area. For example, a prescribed performance function was introduced to complete the error transformation and verify that the error and roll angle were constrained within the prescribed boundary [30]. Ma et al. [31] developed an adaptive neural network method for helicopter systems considering the prescribed performance constraints, which retained the tracking error within a small, prescribed range. In the above studies, PPC was a semi-global result, which depended on the initial conditions. When the system is restarted or parameters are changed, the prescribed function must be reset. The global prescribed performance must be considered to eliminate this dependence and reduce the complexity of the controller in the design process of high performance controllers. Recently, some studies have considered the global prescribed performance in the design of controllers. In [32], adaptive tracking controllers were first introduced to address the finite constraint, infinite time constraint, or even unconstrained problem of a multi-input multi-output (MIMO) system after a period of operation to achieve a global effect. In [33], a new prescribed function was introduced and a global adaptive progressive tracking control algorithm was designed; the performance of the proposed function was verified using a system with an arbitrary relative degree and unknown direction. Chen et al. [34] proposed an iterative adaptive control method based on global and local information, which solved the global prescribed performance affected by the mutation strategy and system parameters. Although the global prescribed performance of nonlinear systems has been significantly improved, the challenging problem of global prescribed performance of 2-DOF helicopter systems must be further investigated.

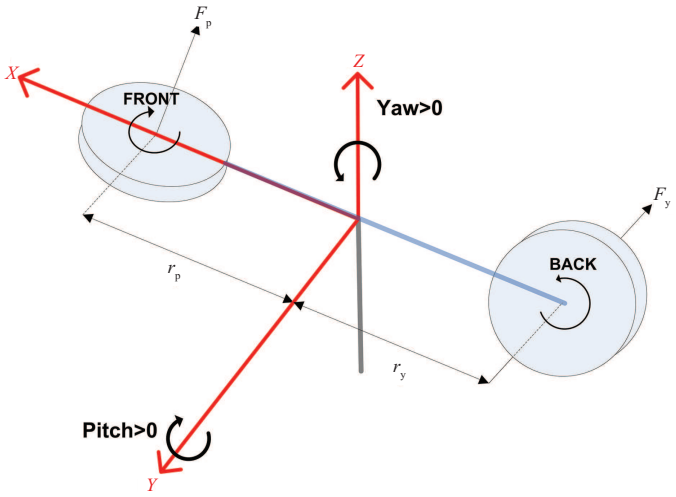

Figure 1 (Color online) Sketch of a 2-DOF helicopter.

Consequently, this study proposes an adaptive NN control for 2-DOF nonlinear helicopter systems affected by an input saturation and a global prescribed performance. The advantages and main contributions of this study are summarized as follows.

(1) Unlike [24,25], in this study, the saturation function is approximated as a smooth nonaffine function to solve the nonlinear problem with input constraints and improve the robustness of the system.

(2) This study proposes a new prescribed function that differs from that presented in [30,31]. As its initial value is not a bounded constant, this property breaks the dependence of the PPC on the initial value and achieves the global prescribed performance of tracking errors.

(3) The rationality and efficacy of the suggested control are verified by conducting simulations and experiments on Quanser's 2-DOF helicopter experiment platform.

The remainder of this paper is structured as follows. Section 2 describes the model of a 2-DOF helicopter system and the related preliminary studies. Section 3 presents the design of an adaptive control based on RBFNN. Section 4 describes the simulation results of the proposed control algorithm. Section 5 describes the experimental platform that was set up to verify the effectiveness of the proposed method. Section 6 draws the conclusion.

2 Problem statement and preliminary study

2.1 Problem statement

The sketch of a 2-DOF helicopter is displayed in Figure 1. The model has two identical propellers. The horizontally placed propeller creates a force $F_{\rm p}$ at a distance $r_{\rm p}$, which generates a torque around the pitch axis to achieve the pitch operation. The vertically placed propeller creates a force $F_{\rm y}$ at a distance $r_{\rm y}$, which generates a torque around the yaw axis to achieve the yaw operation [35]. The helicopter is an MIMO nonlinear system, in which the system input is the voltage of the direct current motor for controlling the propeller. The system output is the pitch and yaw angles.

The 2-DOF helicopter system is modeled using the Lagrangian mechanics and is described as the following dynamic system model [36]:

$$(J_{\rm p}+ml_{\rm cm}^2)\ddot{\theta}=K_{\rm pp}V_{\rm p}+K_{\rm py}V_{\rm y}-mgl_{\rm cm}\cos(\theta)-D_{\rm p}\dot{\theta}-ml_{\rm cm}^2\dot{\phi}^2\sin(\theta)\cos(\theta), \tag{1}$$

$$(J_{\rm y}+ml_{\rm cm}^2\cos^2(\theta))\ddot{\phi}=K_{\rm yp}V_{\rm p}+K_{\rm yy}V_{\rm y}-D_{\rm y}\dot{\phi}+2ml_{\rm cm}^2\dot{\phi}\dot{\theta}\sin(\theta)\cos(\theta), \tag{2}$$

where θ is the pitch angle; ϕ is the yaw angle; m is the mass; $l_{\rm cm}$ is the distance from the center of mass to the rotation point; g is the gravitational acceleration; $K_{\rm pp}$, $K_{\rm py}$, $K_{\rm yp}$, and $K_{\rm yy}$ are the thrust torque constants; $D_{\rm p}$ and $D_{\rm y}$ denote the viscous friction coefficients with respect to the pitch and yaw axes, respectively; and $J_{\rm p}$ and $J_{\rm y}$ represent the rotational inertia around the pitch and yaw axes, respectively.

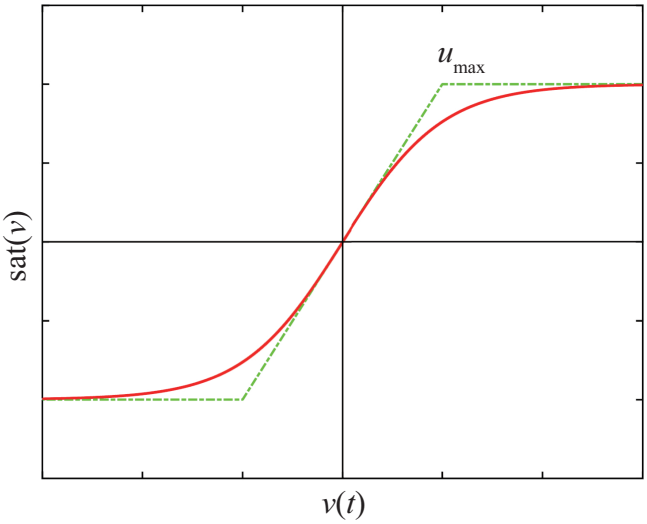

Figure 2 (Color online) The input saturation constraint is approximated by a smooth function $h(v)$ (solid line).

The output vector is defined as $x = [x_1, x_2]^{\mathrm{T}}$, where $x_1 = [\theta, \phi]^{\mathrm{T}}$ and $x_2 = [\dot{\theta}, \dot{\phi}]^{\mathrm{T}}$. It is assumed that the input constraints and global prescribed performance problems exist in the system; thus, Eqs. (1) and (2) can be transformed to simplify the controller design as follows:

$$\dot{x}_1 = x_2, \tag{3}$$

$$\dot{x}_2 = Q(x_1, x_2) + \Delta Q(x_1, x_2) + (P(x_1, x_2) + \Delta P(x_1, x_2))U(v), \tag{4}$$

$$y = x_1, \tag{5}$$

where $\Delta Q(x_1, x_2)$ and $\Delta P(x_1, x_2)$ are the system uncertainties, and $Q(x_1, x_2)$ and $P(x_1, x_2)$ are represented as

$$Q(x_1, x_2) = \begin{bmatrix} \frac{-mgl_{\mathrm{cm}}\cos(\theta) - D_{\mathrm{p}}\dot{\theta} - ml_{\mathrm{cm}}^2\dot{\phi}^2\sin(\theta)\cos(\phi)}{J_{\mathrm{p}} + ml_{\mathrm{cm}}^2} \\ \frac{-D_{\mathrm{y}}\dot{\phi} + 2ml_{\mathrm{cm}}^2\dot{\phi}\dot{\theta}\sin(\theta)\cos(\theta)}{J_{\mathrm{y}} + ml_{\mathrm{cm}}^2\cos^2(\theta)} \end{bmatrix}, \tag{6}$$

$$P(x_1, x_2) = \begin{bmatrix} \frac{K_{\mathrm{pp}}}{J_{\mathrm{p}} + ml_{\mathrm{cm}}^2} & \frac{K_{\mathrm{py}}}{J_{\mathrm{p}} + ml_{\mathrm{cm}}^2} \\ \frac{K_{\mathrm{yp}}}{J_{\mathrm{y}} + ml_{\mathrm{cm}}^2\cos^2(\theta)} & \frac{K_{\mathrm{yy}}}{J_{\mathrm{y}} + ml_{\mathrm{cm}}^2\cos^2(\theta)} \end{bmatrix}. \tag{7}$$

Furthermore, v in (4) is a controller input, and $U(v) = [V_{\mathrm{p}}, V_{\mathrm{y}}]^{\mathrm{T}}$ is a saturated input, formulated as follows:

$$U(v) = \mathrm{sat}(v) = \begin{cases} \mathrm{sign}(v)u_{\max}, & |v| \geqslant u_{\max}, \\ v, & |v| < u_{\max}, \end{cases} \tag{8}$$

with $u_{\max}$ being a known bound of $U(v)$.

Moreover, when $v = u_{\max}$, a sharp angle appears, which is not derivable. To avoid this situation, the input saturation constraint is approximated by a smooth function [37], as shown in Figure 2:

$$\begin{aligned} h(v) &= u_{\max} \times \tanh\left(\frac{v}{u_{\max}}\right) \\ &= u_{\max}\frac{\mathrm{e}^{v/u_{\max}} - \mathrm{e}^{-v/u_{\max}}}{\mathrm{e}^{v/u_{\max}} + \mathrm{e}^{-v/u_{\max}}}. \end{aligned} \tag{9}$$

A deviation $d(v)$ between $U(v)$ and $h(v)$ exists. Consequently, we can obtain

$$d(v) = U(v) - h(v). \tag{10}$$

Owing to the boundedness of sat and tanh functions, we know that the deviation $d(v)$ is a bounded function with bound as

$$|d(v)| = |U(v) - h(v)|$$

$$\begin{aligned}&\leqslant \max\{u_{\max}(1-\tanh(1), u_{\min}(\tanh(1)-1))\}\\&= \bar{d}.\end{aligned} \tag{11}$$

Invoking the mean-value theorem [38], $h(v)$ is expressed as

$$h(v) = h(v_0) + h_{v_\varpi}(v - v_0), \tag{12}$$

where $h_{v_\varpi} = \frac{\partial h(v)}{\partial v}|_{v=v_\varpi}$ and $v_\varpi = \delta v + (1-\delta)v_0$, with $0 < \delta < 1$. Therefore, if $v_0 = 0$, we rewrite (12) as

$$h(v) = h_{v_\varpi} v. \tag{13}$$

Applying (10) and (13) into (4) yields

$$\begin{aligned}\dot{x}_2 &= Q(x_1, x_2) + \Delta Q(x_1, x_2) + (P(x_1, x_2) + \Delta P(x_1, x_2))(h(v) + d(v)),\\&= Q(x_1, x_2) + P(x_1, x_2)h_{v_\varpi} v + L(x, v) + P(x_1, x_2)d(v),\end{aligned} \tag{14}$$

where $L(x, v) = \Delta Q(x_1, x_2) + \Delta P(x_1, x_2)(h_{v_\varpi} v + d(v))$.

Assumption 1 ([39]). Unknown positive constants $\underline{P}$ and $\overline{P}$ exist such that $\underline{P} \leqslant |P| \leqslant \overline{P}$. Without losing generality, $\underline{P} \leqslant P \leqslant \overline{P}$ can be assumed.

Lemma 1 ([40]). The Lyapunov function $V(t)$ is bounded if $V(0)$ is bounded, $V(t)$ is continuous and positive definite, and $\dot{V}(t)$ satisfies the following:

$$\dot{V}(t) \leqslant -\varrho V + Y, \tag{15}$$

where ϱ and Y are positive constants.

Lemma 2 ([41]). The following inequality holds for any $\kappa \in \Re$ and $\varkappa > 0$:

$$0 \leqslant |\kappa| - \kappa\tanh\left(\frac{\kappa}{\varkappa}\right) \leqslant 0.2785\varkappa. \tag{16}$$

2.2 Radial basis function neural network

RBFNNs are frequently used as a tool for controller design of nonlinear systems because of their advantages of approximating arbitrary continuous functions with high accuracy. In this study, the following RBFNN is employed to approximate the unknown and continuous function $f_{nn}(Z) : \mathbb{R}^i \to \mathbb{R}$:

$$f_{nn}(Z) = W^{\mathrm{T}} S(Z), \tag{17}$$

where $Z = [z_1, z_2, \ldots, z_i]^{\mathrm{T}} \in \mathbb{R}^i$ is the input vector, and $W = [w_1, w_2, \ldots, w_l]^{\mathrm{T}} \in \mathbb{R}^l$ is the weight vector, with $l > 1$ denoting the NN node number. In addition, $S(Z) = [s_1(Z), s_2(Z), \ldots, s_l(Z)]^{\mathrm{T}}$ with $s_j(Z)$ are selected as commonly used Gaussian functions, which are represented as

$$s_j(Z) = \exp\left[\frac{-(Z - \Upsilon_j)^{\mathrm{T}}(Z - \Upsilon_j)}{\zeta_j^2}\right], \tag{18}$$

with $\Upsilon_j = [\Upsilon_{j1}, \Upsilon_{j2}, \ldots, \Upsilon_{ji}]^{\mathrm{T}}$ and ζ_j being the center of the receptive field and the width of Gaussian function, respectively.

In general, an RBFNN can smoothly estimate any continuous function over the compact set $\Omega_z \in \mathbb{R}^j$ to any desired accuracy as

$$f(Z) = {W^*}^{\mathrm{T}} S(Z) + \varepsilon(Z), \tag{19}$$

where W^* is an optimal weight vector, and $\varepsilon(Z)$ is an approximation error satisfying $\|\varepsilon(Z)\| \leqslant \bar{\varepsilon}$; furthermore, $\bar{\varepsilon} > 0$ is the bound of ε. The ideal weight vector W^* is defined as

$$W^* = \arg\min_{W \in \mathbb{R}^l} \left\{ \sup_{Z \in \Omega_z} \left| f(Z) - W^{\mathrm{T}} S(Z) \right| \right\}. \tag{20}$$

2.3 Global prescribed performance

We define the tracking error as $e = x_1 - x_d$ with $x_d = [\theta_d, \phi_d]^{\mathrm{T}}$ being a desired trajectory.

2.3.1 *Time-varying scale function*

A time-varying scaling function $\varphi(t)$ is defined with properties as follows:

(1) $\varphi(t)$ is the complex vector space;

(2) $\varphi^{(r)}(t)$, $r = 0, 1, \ldots, n$ is a piecewise smooth derivable and bounded function;

(3) $\varphi(t)$ is monotonically increasing when $t \geqslant 0$ with $\varphi(0) = 1$ and when $t \to \infty$, $\varphi(t) = \frac{1}{g_c}$; g_c is a constant that satisfies $0 < g_c \ll 1$.

2.3.2 *Prescribed performance function*

To avoid the dependence of the prescribed function on the initial value, a new prescribed function related to the function $\varphi(t)$ is designed as follows:

$$I(\omega) = \frac{\sqrt{\vartheta}\omega}{\sqrt{1-\omega^2}}, \tag{21}$$

where $\omega = \frac{1}{\varphi(t)}$ is a time-varying function and ϑ is a constant that satisfies $\vartheta > 0$. Based on these properties of $\varphi(t)$, $\omega(t)$ is strictly monotonically decreasing. In addition, $\omega(0) = 1$ and $\lim_{t\to\infty} \omega(t) = g_c$; thus, the initial value of $I(\omega(0)) = \infty$ can be obtained.

According to (21), the derivative of $I(\omega)$ is expressed as follows:

$$\dot{I}(\omega) = \frac{\sqrt{\vartheta}}{\sqrt{1-\omega^2}(1-\omega^2)}. \tag{22}$$

It is shown that $I(\omega)$ is strictly monotonically increasing when $\omega \in (-1, 1)$ holds for any positive constant ϑ.

Remark 1. Compared with other prescribed functions, the most remarkable feature of the proposed prescribed function $I(\omega)$ is that it eliminates the dependence of the prescribed function on the initial value, which can be infinite. In addition, a global result can be achieved.

2.3.3 *Error transformation*

To eliminate the limitation of the initial value and guarantee the global transient prescribed performance of the system, the tracking error e is transformed and the following normalization function [33] is proposed:

$$\xi(e) = \frac{e}{\sqrt{e^2+\vartheta}}, \tag{23}$$

where ϑ is a constant that satisfies $\vartheta > 0$.

According to (23), the following properties are known:

(1) $\xi(e) \in (-1, 1)$ for any e is strictly monotonical;

(2) when $e \to \infty$, $\xi(e) \to 1$;

(3) when $e \to -\infty$, $\xi(e) \to -1$;

(4) $e = 0 \iff \xi(e) = 0$.

Remark 2. According to (23) and the features of $\xi(e)$, if a constant $\bar{\xi}$ exists that satisfies $|\xi(e)| \leqslant \bar{\xi} < 1$, then $e = \frac{\sqrt{\vartheta}\xi}{\sqrt{1-\xi^2}}$ is bounded.

2.3.4 *Barrier function*

To visualize the performance characteristics as tracking error constraints and achieve tracking error evolution within a prescribed boundary, the following transformation is adopted:

$$\Psi(t) = \varphi(t)\xi(e). \tag{24}$$

Based on the properties of $\varphi(t)$ and $\xi(e(t))$, when $t = 0$, Eq. (24) can be rewritten as

$$\Psi(0) = \varphi(0)\xi(e(0)) = \xi(e(0)) \in (-1, 1), \tag{25}$$

where for any initial conditions, including arbitrary initial trajectory error $e(0)$, we have $|\Psi(0)| < 1$.

Consider the following barrier function:

$$\eta(t) = \frac{\Psi(t)}{1 - \Psi^2(t)}, \tag{26}$$

where $\eta \to \infty$ if and only if $\Psi \to -1$ or $\Psi \to 1$.

2.3.5 *Discussion*

Combined with the above analysis, we suppose that η is bounded for $\forall t \geqslant 0$; then, we can further confirm $|\Psi(t)| < 1$ and $|\Psi(0)| < 1$. Meanwhile, a constant $\mu > 0$ exists satisfying the following:

$$|\Psi(t)| \leqslant \mu < 1 \text{ for } \forall t \geqslant 0. \tag{27}$$

According to (24) and $\omega = \frac{1}{\varphi(t)}$, Eq. (27) can be expressed as follows:

$$-\omega = -\frac{1}{\varphi} < -\frac{\mu}{\varphi} \leqslant \xi \leqslant \frac{\mu}{\varphi} < \frac{1}{\varphi} = \varphi. \tag{28}$$

From the properties of $I(\omega)$, we derive

$$I(-\omega) < I(\xi) < I(\omega). \tag{29}$$

Considering (21) and (23), Eq. (29) can be rewritten as

$$I(-\omega) < \frac{\sqrt{\vartheta}\xi}{\sqrt{1-\xi^2}} = e < I(\omega). \tag{30}$$

According to the derivation of the above conjecture, the boundedness of $\eta(t)$ for $\forall t \geqslant 0$ must be guaranteed to make the tracking error evolve within a prescribed boundary.

Assumption 2 ([42])**.** The desired trajectory x_d is a smooth function of t. In addition, x_d, $\dot{x}_d$, and $\ddot{x}_d$ are continuous and bounded.

3 Neural network control design

Taking the derivative of $\eta(t)$ from (26) results in

$$\dot{\eta} = \frac{1 + \Psi^2}{(1 - \Psi^2)^2}\dot{\Psi}. \tag{31}$$

Based on (24), the time derivative of Ψ yields

$$\dot{\Psi} = \dot{\varphi}\xi + \varphi\dot{\xi}, \tag{32}$$

where the derivative of ξ provided in (23) is derived as

$$\dot{\xi} = \frac{\vartheta\dot{e}}{(e^2 + \vartheta)\sqrt{e^2 + \vartheta}}. \tag{33}$$

Subsequently, Eq. (31) can be deduced as follows:

$$\begin{aligned}\dot{\eta} &= \frac{1 + \Psi^2}{(1 - \Psi^2)^2}\frac{\varphi\vartheta\dot{e}}{(e^2 + \vartheta)\sqrt{e^2 + \vartheta}} + \frac{1 + \Psi^2}{(1 - \Psi^2)^2}\dot{\varphi}\xi \\ &= \rho_1\dot{e} + \rho_2 \\ &= \rho_1(\dot{x_1} - \dot{x_d}) + \rho_2,\end{aligned} \tag{34}$$

where $\rho_1 = \frac{1+\Psi^2}{(1-\Psi^2)^2}\frac{\varphi\vartheta}{(e^2+\vartheta)\sqrt{e^2+\vartheta}}$ and $\rho_2 = \frac{1+\Psi^2}{(1-\Psi^2)^2}\dot{\varphi}\xi$.

Then, we define coordinate transformation:

$$z_1 = \eta, \tag{35}$$

$$z_2 = x_2 - \alpha, \tag{36}$$

where α is a designed virtual control variable.

According to (34)–(36), $\dot{z}_1$ is derived as follows:

$$\dot{z}_1 = \rho_1(z_2 + \alpha - \dot{x}_d) + \rho_2. \tag{37}$$

The Lyapunov function candidate V_1 is chosen as

$$V_1 = \frac{1}{2} z_1^{\mathrm{T}} z_1. \tag{38}$$

Its time derivative is expressed as

$$\dot{V}_1 = z_1^{\mathrm{T}} \dot{z}_1 = z_1^{\mathrm{T}}(\rho_1 z_2 + \rho_1 \alpha - \rho_1 \dot{x}_d + \rho_2). \tag{39}$$

We then design a virtual control variable α as

$$\alpha = -\frac{1}{\rho_1}(k_1 z_1 + \rho_2) + \dot{x}_d, \tag{40}$$

with k_1 being a positive definite diagonal matrix.

The substitution of (40) into (39) results in

$$\dot{V}_1 = -z_1^{\mathrm{T}} k_1 z_1 + z_1^{\mathrm{T}} \rho_1 z_2. \tag{41}$$

According to (40), α is a function of $x_1, x_d, \dot{x_d}, \varphi$, and $\dot{\varphi}$. Differentiating α repeatedly is extremely complicated in the next steps. To overcome this difficulty, the dynamic surface control technology was designed in this study. Introducing the following first-order filter τ and letting α pass through it [43] yields

$$\beta \dot{\tau} + \tau = \alpha, \quad \tau(0) = \alpha(0), \tag{42}$$

where β is a time constant of the filter.

Moreover, $\gamma = \tau - \alpha$ is defined. Subsequently, we obtain

$$\begin{aligned} \dot{\gamma} &= \dot{\tau} - \dot{\alpha} \\ &= -\frac{\gamma}{\beta} + \left(-\frac{\partial \alpha}{\partial x_1}\dot{x}_1 - \frac{\partial \alpha}{\partial x_d}\dot{x}_d - \frac{\partial \alpha}{\partial \dot{x}_d}\ddot{x}_d - \frac{\partial \alpha}{\partial \varphi}\dot{\varphi} - \frac{\partial \alpha}{\partial \dot{\varphi}}\ddot{\varphi} \right) \\ &= -\frac{\gamma}{\beta} + M\left(x_1, x_d, \dot{x}_d, \varphi, \dot{\varphi}\right), \end{aligned} \tag{43}$$

where M is a continuous function vector about $\mho(x_1, x_d, \dot{x}_d, \varphi, \dot{\varphi})$. Based on the continuous property, the set $\mho(\cdot)$ is compact for certain initial conditions. A maximum $\bar{M}$ of $M(\cdot)$ with $\|M\| \leqslant \bar{M}$ on set $\mho(\cdot)$ exists.

Therefore, Eq. (43) becomes

$$\dot{\gamma} \leqslant -\frac{\gamma}{\beta} + \bar{M}. \tag{44}$$

As for (14), because $L(x, v)$ is unknown and difficult to determine, we employ the RBFNN to approximate this uncertainty term as follows:

$$L(x, v) = {W^*}^{\mathrm{T}} S(Z) + \varepsilon(Z), \tag{45}$$

where W^* represents an ideal weight vector that satisfies $\tilde{W} = \hat{W} - W^*$; $S(Z)$ is a radial basis vector with Gaussian function; $Z = [x_1^{\mathrm{T}}, x_2^{\mathrm{T}}, x_d^{\mathrm{T}}, \dot{x}_d^{\mathrm{T}}, v^{\mathrm{T}}]^{\mathrm{T}}$ is the input variable to the RBFNN; and $\varepsilon(Z)$ describes an estimation error that satisfies $\|\varepsilon(Z)\| \leqslant \bar{\varepsilon}$, where $\bar{\varepsilon} > 0$ is a constant.

Substituting (14) and (45) into the time derivative of (36) yields

$$\dot{z}_2 = \dot{x}_2 - \dot{\alpha}$$

$$= Q + Ph_{v_\varpi} v + W^{*\mathrm{T}} S(Z) + \varepsilon(Z) + \Xi - \dot{\alpha}, \tag{46}$$

where $\Xi = P(x_1, x_2)d(v)$. According to Assumption 1 and (11), it is observed that Ξ is bounded. Subsequently, $\|\Xi\| < \bar{\Xi}$ can be derived, where $\bar{\Xi} > 0$ is an unknown constant. Subsequently, $\tilde{\bar{\Xi}} = \hat{\bar{\Xi}} - \bar{\Xi}$ is defined.

The Lyapunov function candidate is selected as

$$V_2 = V_1 + \frac{1}{2} z_2^{\mathrm{T}} z_2. \tag{47}$$

We differentiate (47) to obtain

$$\dot{V}_2 = \dot{V}_1 + z_2^{\mathrm{T}} \dot{z}_2. \tag{48}$$

Substituting (46) into (48) yields

$$\dot{V}_2 = \dot{V}_1 + z_2^{\mathrm{T}} (Q + Ph_{v_\varpi} v + \Xi + L - \dot{\alpha}). \tag{49}$$

Subsequently, we construct the controller as follows:

$$v = (Ph_{v_\varpi})^{-1} \left[-Q - \hat{W}^{\mathrm{T}} S(Z) - \rho_1 z_1 - k_2 z_2 - \tanh\left(\frac{z_2}{\epsilon}\right) \hat{\bar{\Xi}} + \dot{\tau} \right], \tag{50}$$

where k_2 is a positive constant matrix.

We then define updating laws of $\hat{W}$ and $\hat{\bar{\Xi}}$ as

$$\dot{\hat{W}} = \Gamma_w \left[S(Z) z_2^{\mathrm{T}} - \sigma_w \hat{W} \right], \tag{51}$$

$$\dot{\hat{\bar{\Xi}}} = \psi_{\bar{\Xi}} \left[z_2^{\mathrm{T}} \tanh\left(\frac{z_2}{\epsilon}\right) - \sigma_{\bar{\Xi}} \hat{\bar{\Xi}} \right], \tag{52}$$

where $\Gamma_w = \Gamma_w^{\mathrm{T}} \in \mathbb{R}^{l \times l}$, $\Gamma_w > 0$, and $\psi_{\bar{\Xi}} > 0$. In addition, σ_w and $\sigma_{\bar{\Xi}}$ are the designed positive constants.

Substituting (45) and (50) into (49) yields

$$\begin{aligned} \dot{V}_2 =& \dot{V}_1 + z_2^{\mathrm{T}} \left[-\hat{W}^{\mathrm{T}} S(Z) - \rho_1 z_1 - k_2 z_2 - \tanh\left(\frac{z_2}{\epsilon}\right) \hat{\bar{\Xi}} \right. \\ & \left. + \dot{\tau} + \Xi + W^{*\mathrm{T}} S(Z) + \varepsilon(Z) - \dot{\alpha} \right] \\ =& - z_1^{\mathrm{T}} k_1 z_1 - z_2^{\mathrm{T}} k_2 z_2 + z_2^{\mathrm{T}} \Xi - z_2^{\mathrm{T}} \tilde{W}^{\mathrm{T}} S(Z) + z_2^{\mathrm{T}} \varepsilon(Z) \\ & + z_2^{\mathrm{T}} (\dot{\tau} - \dot{\alpha}) - z_2^{\mathrm{T}} \tanh\left(\frac{z_2}{\epsilon}\right) \hat{\bar{\Xi}}. \end{aligned} \tag{53}$$

We select the Lyapunov function candidate as

$$V_3 = V_2 + \mathrm{tr}\left\{ \frac{1}{2} \tilde{W}^{\mathrm{T}} \Gamma_w^{-1} \tilde{W} \right\} + \frac{1}{2\psi_{\bar{\Xi}}} \tilde{\bar{\Xi}}^2 + \frac{1}{2} \gamma^{\mathrm{T}} \gamma. \tag{54}$$

We thus derive $\dot{V}_3$ as

$$\begin{aligned} \dot{V}_3 =& \dot{V}_2 + \mathrm{tr}\left\{ \tilde{W}^{\mathrm{T}} \Gamma_w^{-1} \dot{\hat{W}} \right\} + \frac{1}{\psi_{\bar{\Xi}}} \tilde{\bar{\Xi}} \dot{\hat{\bar{\Xi}}} + \gamma^{\mathrm{T}} \dot{\gamma} \\ =& - z_1^{\mathrm{T}} k_1 z_1 - z_2^{\mathrm{T}} k_2 z_2 - \sigma_w \mathrm{tr}\left\{ \tilde{W}^{\mathrm{T}} \hat{W} \right\} - \sigma_{\bar{\Xi}} \tilde{\bar{\Xi}} \hat{\bar{\Xi}} + (z_2^{\mathrm{T}} + \gamma^{\mathrm{T}}) \left(-\frac{\gamma}{\beta} + M \right) \\ & + z_2^{\mathrm{T}} \varepsilon + z_2^{\mathrm{T}} \Xi - z_2^{\mathrm{T}} \tanh\left(\frac{z_2}{\epsilon}\right) \hat{\bar{\Xi}} + \tilde{\bar{\Xi}} z_2^{\mathrm{T}} \tanh\left(\frac{z_2}{\epsilon}\right). \end{aligned} \tag{55}$$

We consider the following inequalities:

$$z_2^{\mathrm{T}} \Xi \leqslant \bar{\Xi} \sum_{k=1}^{2} |z_{2k}|, \tag{56}$$

$$z_2^{\mathrm{T}}\tanh\left(\frac{z_2}{\epsilon}\right)=\sum_{k=1}^{2}\left(z_{2k}\tanh\left(\frac{z_{2k}}{\epsilon}\right)\right). \tag{57}$$

Applying Lemma 2, we have

$$\sum_{k=1}^{2}|z_{2k}|-\sum_{k=1}^{2}\left(z_{2k}\tanh\left(\frac{z_{2k}}{\epsilon}\right)\right)\leqslant 0.557\epsilon. \tag{58}$$

Substituting (58) into (55) yields

$$\begin{aligned}\dot{V}_3\leqslant&-z_1^{\mathrm{T}}k_1z_1-z_2^{\mathrm{T}}k_2z_2-\sigma_w\mathrm{tr}\left\{\tilde{W}^{\mathrm{T}}\hat{W}\right\}-\sigma_{\bar{\Xi}}\tilde{\bar{\Xi}}\hat{\bar{\Xi}}\\&+(z_2^{\mathrm{T}}+\gamma^{\mathrm{T}})\left(-\frac{\gamma}{\beta}+M\right)+z_2^{\mathrm{T}}\varepsilon+0.557\epsilon\bar{\Xi}.\end{aligned} \tag{59}$$

Using the Young's inequality results in

$$z_2^{\mathrm{T}}\varepsilon\leqslant\frac{1}{2}z_2^{\mathrm{T}}z_2+\frac{1}{2}\left\|\varepsilon\right\|^2\leqslant\frac{1}{2}z_2^{\mathrm{T}}z_2+\frac{1}{2}\bar{\varepsilon}^2, \tag{60}$$

$$-\frac{z_2^{\mathrm{T}}\gamma}{\beta}\leqslant\frac{z_2^{\mathrm{T}}z_2}{2\beta}+\frac{\gamma^{\mathrm{T}}\gamma}{2\beta}, \tag{61}$$

$$z_2^{\mathrm{T}}M\leqslant\frac{1}{2}z_2^{\mathrm{T}}z_2+\frac{1}{2}\left\|M\right\|^2\leqslant\frac{1}{2}z_2^{\mathrm{T}}z_2+\frac{1}{2}\bar{M}^2, \tag{62}$$

$$\gamma^{\mathrm{T}}M\leqslant\frac{1}{2}\gamma^{\mathrm{T}}\gamma+\frac{1}{2}\left\|M\right\|^2\leqslant\frac{1}{2}\gamma^{\mathrm{T}}\gamma+\frac{1}{2}\bar{M}^2, \tag{63}$$

$$-\sigma_w\mathrm{tr}\left\{\tilde{W}^{\mathrm{T}}\hat{W}\right\}\leqslant-\frac{\sigma_w}{2}\left\|\tilde{W}\right\|^2+\frac{\sigma_w}{2}\left\|W^*\right\|^2, \tag{64}$$

$$-\sigma_{\bar{\Xi}}\tilde{\bar{\Xi}}\hat{\bar{\Xi}}\leqslant-\frac{\sigma_{\bar{\Xi}}}{2}\tilde{\bar{\Xi}}^2+\frac{\sigma_{\bar{\Xi}}}{2}\bar{\Xi}^2. \tag{65}$$

Substituting (60)–(65) into (55) gains

$$\begin{aligned}\dot{V}_3\leqslant&-z_1^{\mathrm{T}}k_1z_1-z_2^{\mathrm{T}}\left(k_2-I-\frac{1}{2\beta}\right)z_2-\frac{\sigma_w}{2}\left\|\tilde{W}\right\|^2-\frac{\sigma_{\bar{\Xi}}}{2}\tilde{\bar{\Xi}}^2-\left[\frac{1}{2\beta}-\frac{1}{2}I\right]\gamma^{\mathrm{T}}\gamma\\&+\frac{1}{2}\overline{\varepsilon}+\bar{M}^2+\frac{1}{2}\sigma_w\left\|W^*\right\|^2+\frac{1}{2}\sigma_{\bar{\Xi}}\bar{\Xi}^2+0.557\epsilon\bar{\Xi}\\\leqslant&-\varrho V_3+Y,\end{aligned} \tag{66}$$

where

$$\begin{aligned}\varrho=\min\Bigg\{&2\lambda_{\min}(k_1),2\lambda_{\min}\left(k_2-I-\frac{1}{2\beta}\right),\\&\frac{\sigma_w}{\lambda_{\max}(\Gamma_w^{-1})},2\lambda_{\min}\psi_{\bar{\Xi}}\left(\frac{\sigma_{\bar{\Xi}}}{2}\right),2\lambda_{\min}\left[\frac{1}{2\beta}-\frac{1}{2}I\right]\Bigg\},\end{aligned} \tag{67}$$

$$Y=\frac{1}{2}\overline{\varepsilon}+\bar{M}^2+\frac{1}{2}\sigma_w\left\|W^*\right\|^2+\frac{1}{2}\sigma_{\bar{\Xi}}\bar{\Xi}^2+0.557\epsilon\bar{\Xi}. \tag{68}$$

To guarantee $\varrho>0$, k_1, k_2, and β are chosen as

$$\lambda_{\min}(k_1)>0,\ \lambda_{\min}\left(k_2-I-\frac{1}{2\beta}\right)>0,\ \lambda_{\min}\left[\frac{1}{2\beta}-\frac{1}{2}I\right]>0. \tag{69}$$

Theorem 1. For the 2-DOF helicopter system described by (3) and (14), under the control law (50) and updating laws (51) and (52), the globally uniformly bounded in the closed-loop system is proven. According to (66), tracking errors z_1 and z_2 and weight errors $\tilde{W}$ and $\tilde{\bar{\Xi}}$ are globally bounded by employing Lemma 1.

Table 1 System parameters

Parameter	Value	Unit	Parameter	Value	Unit
J_{p}	0.0215	$\mathrm{kg}\cdot\mathrm{m}^2$	D_{y}	0.0220	N/V
J_{y}	0.0237	$\mathrm{kg}\cdot\mathrm{m}^2$	K_{pp}	0.0011	$\mathrm{N}\cdot\mathrm{m/V}$
l_{cm}	0.0025	m	K_{py}	0.0021	$\mathrm{N}\cdot\mathrm{m/V}$
m	1.0750	kg	K_{yp}	−0.0027	$\mathrm{N}\cdot\mathrm{m/V}$
D_{p}	0.0071	N/V	K_{yy}	0.0022	$\mathrm{N}\cdot\mathrm{m/V}$

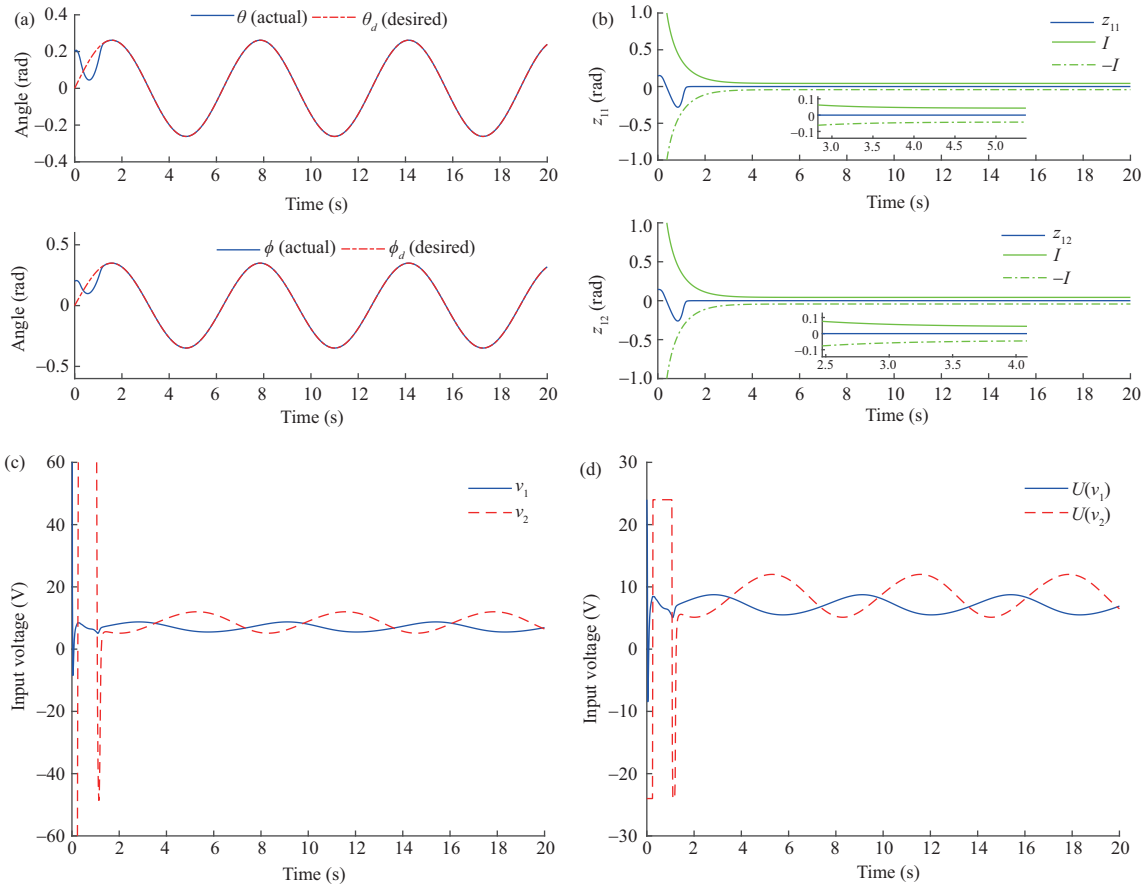

Figure 3 (Color online) Simulation results considering the global prescribed performance. (a) θ and ϕ tracking control results; (b) tracking errors z_{11} and z_{12}; (c) control inputs v_1 and v_2; (d) control input saturations $U(v_1)$ and $U(v_2)$.

Proof. Multiplying both sides of (66) by $\mathrm{e}^{\varrho t}$ provides

$$\frac{\mathrm{d}}{\mathrm{d}t}(V_3\mathrm{e}^{\varrho t}) \leqslant Y\mathrm{e}^{\varrho t}. \tag{70}$$

Integrating the inequality (70) yields

$$0 \leqslant V_3 \leqslant \left(V_3(0) - \frac{Y}{\varrho}\right)\mathrm{e}^{-\varrho t} + \frac{Y}{\varrho}. \tag{71}$$

Moreover, Eq. (71) shows that V_3 is convergent, and $\lim_{t\to\infty} V_3 = \frac{Y}{\varrho}$. According to the properties of η, Ψ, and ξ, as expressed in (26), (24), and (23), respectively, we derive $\lim_{t\to\infty} e(t) = 0$, which proves that the closed-loop signals z_1, z_2, $\tilde{W}$, and $\tilde{\tilde{\Xi}}$ are bounded; in addition, it guarantees the global prescribed performance of the system. Therefore, the proof is completed.

Remark 3. Because the typical prescribed performance constraint control comparison depends on the output and initial values of the desired trajectory, it is hemispherical in nature. A new prescribed function is constructed to guarantee the global transient prescribed performance of the system and address the relationship between the controller and initial parameter values.

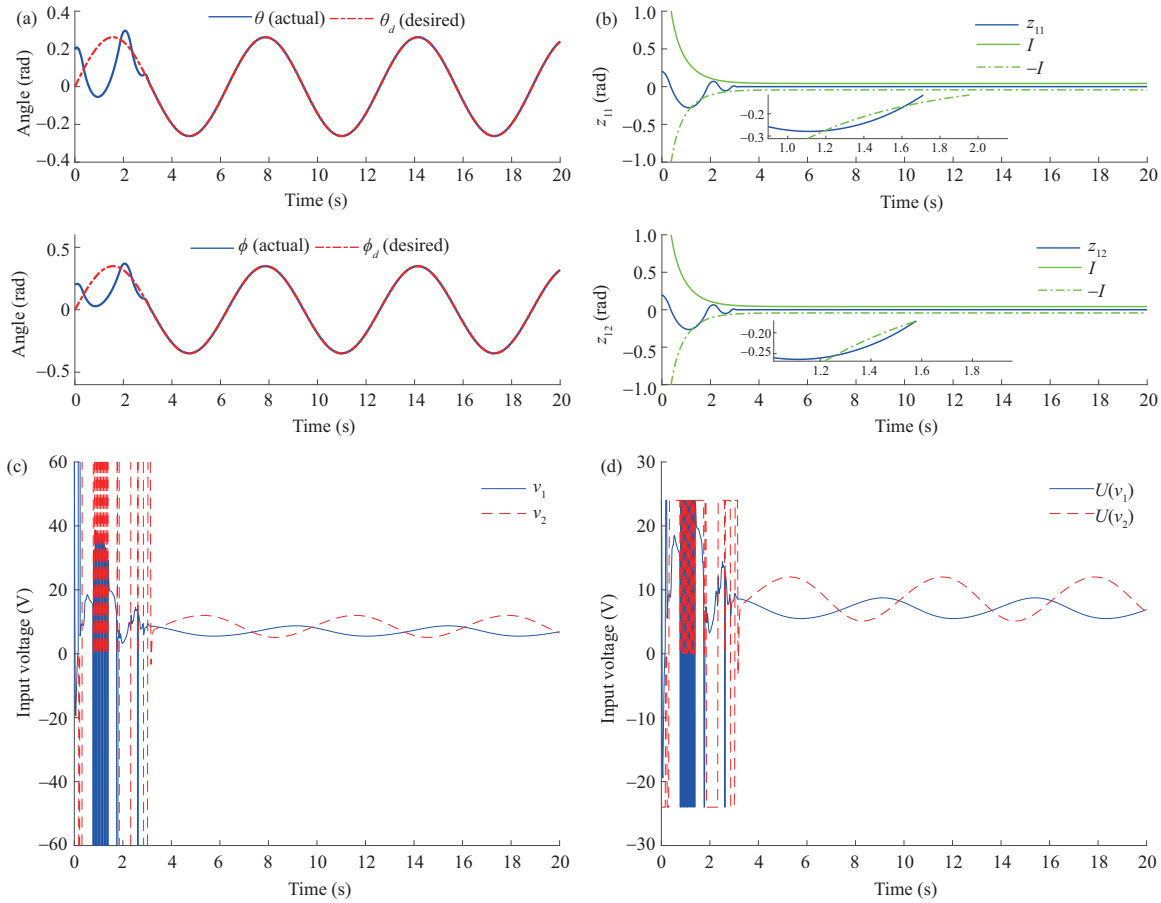

Figure 4 (Color online) Simulation results without the global prescribed performance. (a) θ and ϕ tracking control results; (b) tracking errors z_{11} and z_{12}; (c) control inputs v_1 and v_2; (d) control input saturations $U(v_1)$ and $U(v_2)$.

4 Simulation results

Simulations are used to validate the performance of the proposed control. The 2-DOF helicopter's structural parameters for simulations are listed in Table 1.

We set the 2-DOF helicopter trajectory tracking command as the continuous-time expected trajectory. The expected attitude trajectory is set as $x_d = [\frac{\pi}{12}\sin(t), \frac{\pi}{9}\sin(t)]^{\mathrm{T}}$, where $t \in [0, 20]$. The voltage of the DC motor is ± 24 V.

In addition, the initial state of the helicopter flight control simulation is expressed as $x_1 = [0.2, 0.2]^{\mathrm{T}}$ and $x_2 = [0.2, 0.2]^{\mathrm{T}}$. The control gains are chosen as $k_1 = \mathrm{diag}[18, 18]$ and $k_2 = \mathrm{diag}[18, 18]$. The design parameters of updating laws are chosen as $\Gamma_w = 15I_{32\times 32}$, $\psi_{\Xi} = 2I_{2\times 2}$, $\sigma_w = 0.01$, and $\sigma_{\Xi} = 0.01$. Other design parameters are selected as $k_m = 0.03$, $\vartheta = 2$, $\beta = 0.01$, and $\epsilon = 0.45$. The NN has 32 nodes and the variance is 16. The initial weight of the NN is set to zero. The time-varying scaling function $\varphi(t)$ is selected as $\varphi(t) = \frac{1}{(1-k_m)\mathrm{e}^{-1.5t}+k_m}$.

4.1 Simulation with global prescribed performance

Figure 3 depicts the simulation results considering the global performance of the system. Figure 3(a) shows the tracking performance of pitch angle θ and yaw angle ϕ. The desired trajectory is tracked in approximately 2 s and a satisfactory tracking performance is obtained. Figure 3(b) depicts the tracking error of attitude angles. The tracking error under this control algorithm converges to zero extremely quickly. Figure 3(c) presents the voltage of the control input. Figure 3(d) shows the input voltage with constraints. The control input is maintained at a safe voltage of 24 V under the saturation constraint. After considering the saturation constraint, the control input exhibits a satisfactory input performance at a safe voltage of a maximum of 24 V.

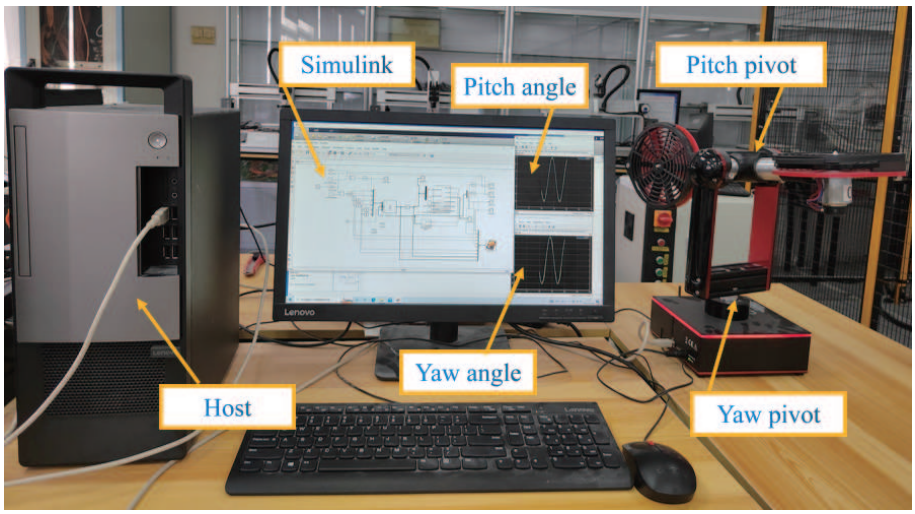

Figure 5 (Color online) 2-DOF helicopter test platform.

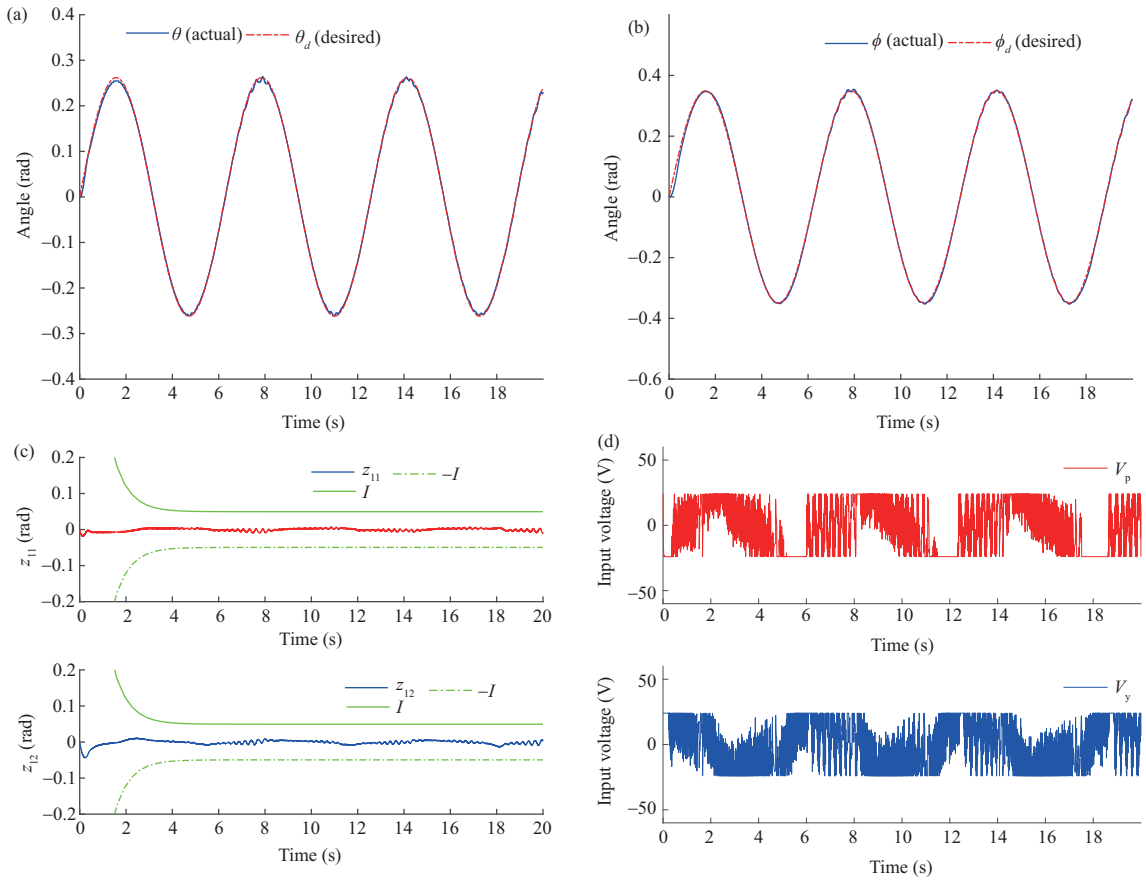

Figure 6 (Color online) Experimental results considering the global prescribed performance. (a) θ tracking control result; (b) ϕ tracking control result; (c) tracking errors z_{11} and z_{12}; (d) control inputs $V_{\rm p}$ and $V_{\rm y}$.

4.2 Simulation without global prescribed performance

We compared the simulation results with and without global prescribed performance to illustrate the rationality of the proposed control; the results are displayed in Figure 4. The tracking responses of pitch angle θ and yaw angle ϕ in Figure 4(a) show that θ and ϕ eventually stably track the expected trajectory with lower performance than that shown in Figure 3(a). According to Figure 4(b), the tracking error significantly oscillates and violates the preset prescribed performance I and $-I$. Figures 4(c) and (d)

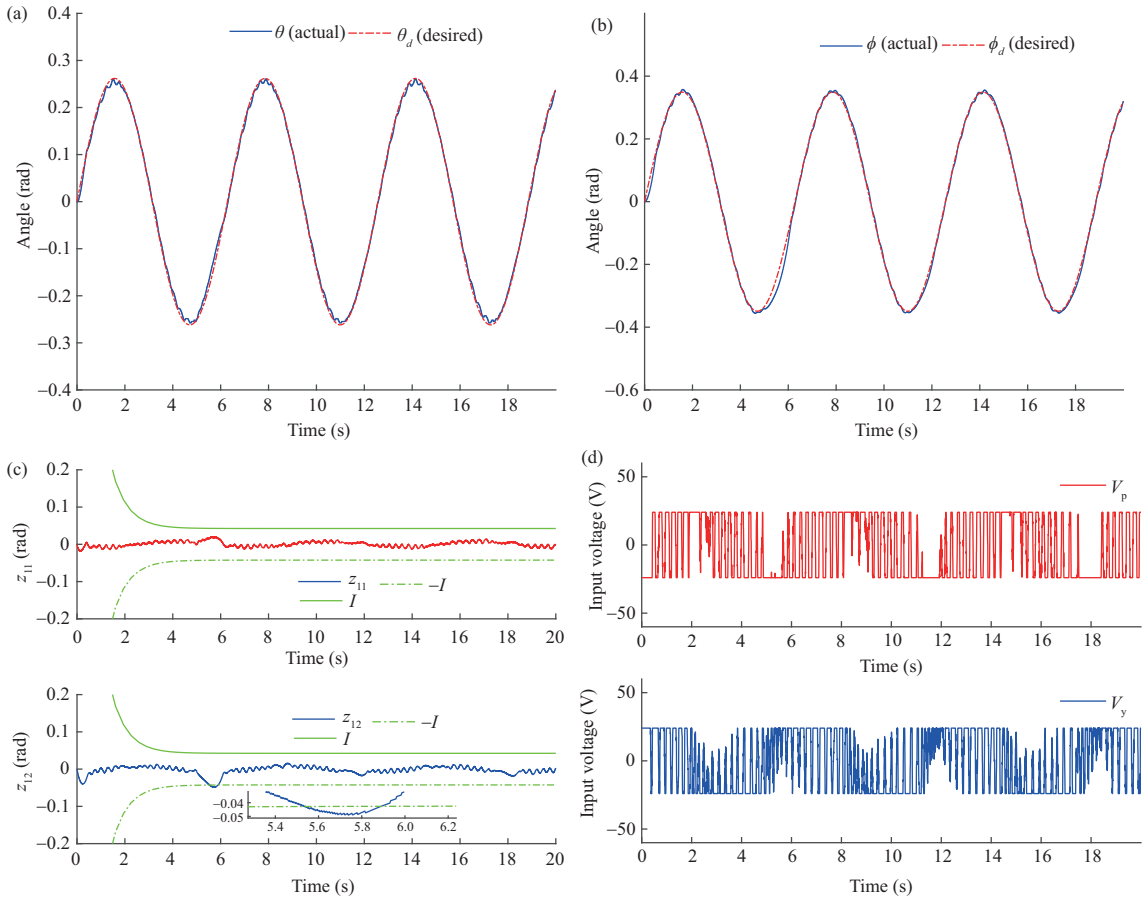

Figure 7 (Color online) Experimental results without the global prescribed performance. (a) θ tracking control result; (b) ϕ tracking control result; (c) tracking errors z_{11} and z_{12}; (d) control inputs $V_{\rm p}$ and $V_{\rm y}$.

represent the control input and input saturation response of the system.

Consequently, the proposed method is effective for the stability control of a 2-DOF helicopter system considering input constraints and global prescribed performance.

5 Experimental results

An experimental platform on Quanser's 2-DOF helicopter is constructed to further demonstrate the feasibility and efficacy of the proposed control, as shown in Figure 5. The same parameters are chosen as discussed in Section 4. The experiments are conducted with and without global prescribed performance.

5.1 Experiments with global prescribed performance

Figure 6 portrays the experimental results considering the global prescribed performance. Figures 6(a) and (b) depict the pitch angle θ and yaw angle ϕ responses of the helicopter. The results reveal a reasonable tracking performance. Figure 6(c) depicts the tracking errors of pitch and yaw angles; it is obvious that the error is maintained within a prescribed, small, compact range I and $-I$, and the tracking effect is satisfactory. Figure 6(d) represents the evolution of the control input, which exhibits a reasonable trajectory performance.

5.2 Experiments without global prescribed performance

Figure 7 presents a comparison of the experimental results without considering the global prescribed performance. Figures 7(a) and (b) illustrate the evolution of the pitch and yaw angles, respectively. It can be seen that the tracking speed is slower around the corner. Figure 7(c) depicts the effect of the tracking error. The error oscillation amplitude is large, and maintaining the tracking error of each

attitude within the preset prescribed performance cannot always be guaranteed. Figure 7(d) depicts the evolution of the control input, which presents a poor response performance.

Consequently, the experiments with the global prescribed performance achieve better tracking performance, ensuring that the error does not violate the prescribed performance and quickly converges to zero. In addition, the input voltage exhibits a reasonable performance. These results validate the stability, rationality, and efficacy of the developed adaptive NN control for a 2-DOF helicopter system considering the input constraints and global prescribed performance.

6 Conclusion

This study developed an adaptive NN control for 2-DOF nonlinear helicopter systems considering the input constraints and global prescribed performance. An RBFNN was used to approximate the system uncertainties. To solve the nonlinear input constraint, the smooth hyperbolic tangent function was introduced to approximate the constraint function. Additionally, a new prescribed function was proposed, and the constraint problem was transformed into an unconstrained error problem using the normalization and barrier function transformation. Furthermore, the Lyapunov stability analysis proved that the system was globally uniformly bounded. Finally, the simulation and experimental results were compared to verify the effectiveness and stability of the proposed control.

Acknowledgements This work was supported in part by National Key Research and Development Program of China (Grant No. 2023YFB4706400), National Natural Science Foundation of China (Grant Nos. 62273112, 62225304, 92267203), Science and Technology Major Project of Guangzhou (Grant No. 202007030006), Science and Technology Planning Project of Guangzhou (Grant Nos. 202201020185, 2023A03J0120), Program for Guangdong Introducing Innovative and Entrepreneurial Teams (Grant No. 2019ZT08X214), and Guangzhou University Research Project (Grant No. RC2023037).

References

1 Maini P, Tokekar P, Sujit P B. Visual monitoring of points of interest on a 2.5D terrain using a UAV with limited field-of-view constraint. IEEE Trans Aerosp Electron Syst, 2021, 57: 3661–3672
2 Sheng M, Zhao C X, Liu J Y, et al. Energy-efficient trajectory planning and resource allocation in UAV communication networks under imperfect channel prediction. Sci China Inf Sci, 2022, 65: 222301
3 Xia S D, Tao X F, Li N, et al. Physical layer authentication in UAV-enabled relay networks based on manifold learning. Sci China Inf Sci, 2022, 65: 222302
4 Lotufo M A, Colangelo L, Novara C. Control design for UAV quadrotors via embedded model control. IEEE Trans Contr Syst Technol, 2020, 28: 1741–1756
5 Zhao Z J, He W T, Zhang F K, et al. Deterministic learning from adaptive neural network control for a 2-DOF helicopter system with unknown backlash and model uncertainty. IEEE Trans Ind Electron, 2023, 70: 9379–9389
6 Kumar E V, Raaja G S, Jerome J. Adaptive PSO for optimal LQR tracking control of 2 DoF laboratory helicopter. Appl Soft Computing, 2016, 41: 77–90
7 Luo B, Wu H-N, Huang T W. Optimal output regulation for model-free quanser helicopter with multistep Q-learning. IEEE Trans Ind Electron, 2018, 65: 4953–4961
8 Subramanian R G, Elumalai V K. Robust MRAC augmented baseline LQR for tracking control of 2 DoF helicopter. Robotics Autonomous Syst, 2016, 86: 70–77
9 Zou Y, Huo W. Nonlinear robust controller for miniature helicopters without singularity. IEEE Trans Aerosp Electron Syst, 2017, 53: 1402–1411
10 Castellanos J E R, Ballesteros J E C. Implementation of a direct fuzzy controller applied to a helicopter with one degree of freedom. IEEE Latin Am Trans, 2019, 17: 1808–1814
11 Wu Y H, Hu K J, Sun X M, et al. Nonlinear control of quadrotor for fault tolerance: a total failure of one actuator. IEEE Trans Syst Man Cybern Syst, 2021, 51: 2810–2820
12 Zerari N, Chemachema M, Essounbouli N. Neural network based adaptive tracking control for a class of pure feedback nonlinear systems with input saturation. IEEE CAA J Autom Sin, 2019, 6: 278–290
13 Zhang T, Wang X H, Xu X M, et al. GCB-Net: graph convolutional broad network and its application in emotion recognition. IEEE Trans Affective Comput, 2022, 13: 379–388
14 Yang H J, Liu J K. An adaptive RBF neural network control method for a class of nonlinear systems. IEEE CAA J Autom Sin, 2018, 5: 457–462
15 Lin G H, Li H Y, Ahn C K, et al. Event-based finite-time neural control for human-in-the-loop UAV attitude systems. IEEE Trans Neural Netw Learn Syst, 2022, 34: 10387–10397
16 Yang X B, Zheng X L. Adaptive NN backstepping control design for a 3-DOF helicopter: theory and experiments. IEEE Trans Ind Electron, 2020, 67: 3967–3979
17 Zhao Z J, Zhang J, Liu Z J, et al. Adaptive neural network control of an uncertain 2-DOF helicopter with unknown backlash-like hysteresis and output constraints. IEEE Trans Neural Netw Learn Syst, 2022, 34: 10018–10027
18 Zhao Z J, He W T, Yang J F, et al. Adaptive neural network control of an uncertain 2-DOF helicopter system with input backlash and output constraints. Neural Comput Applic, 2022, 34: 18143–18154
19 Tan S P, Guo J, Zhao Y L, et al. Adaptive control with saturation-constrainted observations for drag-free satellites - a set-valued identification approach. Sci China Inf Sci, 2021, 64: 202202
20 Zhang G Q, Yao M Q, Shan Q H, et al. Observer-based asynchronous self-triggered control for a dynamic positioning ship with the hysteresis input. Sci China Inf Sci, 2022, 65: 212206
21 Wang Y Y, Li S Y, Zheng Y. Model predictive control with input disturbance and guaranteed Lyapunov stability for controller approximation. Sci China Inf Sci, 2022, 65: 192205

22 Zhao T, Liu Y Y, Li Z J, et al. Adaptive control and optimization of mobile manipulation subject to input saturation and switching constraints. IEEE Trans Automat Sci Eng, 2019, 16: 1543–1555
23 Sedghi F, Arefi M M, Abooee A, et al. Adaptive robust finite-time nonlinear control of a typical autonomous underwater vehicle with saturated inputs and uncertainties. IEEE ASME Trans Mechatron, 2021, 26: 2517–2527
24 Zhang J, Yang Y B, Zhao Z J, et al. Adaptive neural network control of a 2-DOF helicopter system with input saturation. Int J Control Autom Syst, 2023, 21: 318–327
25 Huang H F, He W, Wang J B, et al. An all servo-driven bird-like flapping-wing aerial robot capable of autonomous flight. IEEE ASME Trans Mechatron, 2022, 27: 5484–5494
26 Bechlioulis C P, Rovithakis G A. Robust adaptive control of feedback linearizable MIMO nonlinear systems with prescribed performance. IEEE Trans Automat Contr, 2008, 53: 2090–2099
27 Yang Y, Si X F, Yue D, et al. Time-varying formation tracking with prescribed performance for uncertain nonaffine nonlinear multiagent systems. IEEE Trans Automat Sci Eng, 2021, 18: 1778–1789
28 Zhang F K, Wu W M, Wang C. Pattern-based learning and control of nonlinear pure-feedback systems with prescribed performance. Sci China Inf Sci, 2023, 66: 112202
29 Liang J C, Chen Y J, Wu Y N, et al. Adaptive prescribed performance control of unmanned aerial manipulator with disturbances. IEEE Trans Autom Sci Eng, 2023, 20: 1804–1814
30 Hu C, Wang Z F, Qin Y C, et al. Lane keeping control of autonomous vehicles with prescribed performance considering the rollover prevention and input saturation. IEEE Trans Intell Transp Syst, 2020, 21: 3091–3103
31 Ma G, Wu H Y, Zhao Z J, et al. Adaptive neural network control of a non-linear two-degree-of-freedom helicopter system with prescribed performance. IET Control Theor & Appl, 2023, 17: 1789–1799
32 Kong L H, He W, Liu Z J, et al. Adaptive tracking control with global performance for output-constrained MIMO nonlinear systems. IEEE Trans Automat Contr, 2023, 68: 3760–3767
33 Zhao K, Song Y D, Chen C L P, et al. Adaptive asymptotic tracking with global performance for nonlinear systems with unknown control directions. IEEE Trans Automat Contr, 2022, 67: 1566–1573
34 Chen D B, Zou F, Lu R Q, et al. Backtracking search optimization algorithm based on knowledge learning. Inf Sci, 2019, 473: 202–226
35 Ouyang Y, Dong L, Xue L, et al. Adaptive control based on neural networks for an uncertain 2-DOF helicopter system with input deadzone and output constraints. IEEE CAA J Autom Sin, 2019, 6: 807–815
36 Xin Y, Qin Z-C, Sun J-Q. Input-output tracking control of a 2-DOF laboratory helicopter with improved algebraic differential estimation. IEEE Trans Autom Sci Eng, 2019, 116: 843–857
37 Wen C Y, Zhou J, Liu Z T, et al. Robust adaptive control of uncertain nonlinear systems in the presence of input saturation and external disturbance. IEEE Trans Automat Contr, 2011, 56: 1672–1678
38 Cao L, Ren H R, Meng W, et al. Distributed event triggering control for six-rotor UAV systems with asymmetric time-varying output constraints. Sci China Inf Sci, 2021, 64: 172213
39 Lv M L, Yu W W, Baldi S. The set-invariance paradigm in fuzzy adaptive DSC design of large-scale nonlinear input-constrained systems. IEEE Trans Syst Man Cybern Syst, 2021, 51: 1035–1045
40 Liu Y J, Chen H. Adaptive sliding mode control for uncertain active suspension systems with prescribed performance. IEEE Trans Syst Man Cybern Syst, 2021, 51: 6414–6422
41 Kong L H, Lai Q C, Ouyang Y C, et al. Neural learning control of a robotic manipulator with finite-time convergence in the presence of unknown backlash-like hysteresis. IEEE Trans Syst Man Cybern Syst, 2022, 52: 1916–1927
42 Liu Z, Lu K X, Lai G Y, et al. Indirect fuzzy control of nonlinear systems with unknown input and state hysteresis using an alternative adaptive inverse. IEEE Trans Fuzzy Syst, 2021, 29: 500–514
43 Wang C L, Lin Y. Adaptive dynamic surface control for linear multivariable systems. Automatica, 2010, 46: 1703–1711